APPLIED SCIENCES AND ENGINEERING

Pathways and challenges for efficient solar-thermal desalination

Zhangxin Wang[1,2], Thomas Horseman[1], Anthony P. Straub[3], Ngai Yin Yip[4], Deyu Li[5], Menachem Elimelech[2]*, Shihong Lin[1,6]*

Solar-thermal desalination (STD) is a potentially low-cost, sustainable approach for providing high-quality fresh water in the absence of water and energy infrastructures. Despite recent efforts to advance STD by improving heat-absorbing materials and system designs, the best strategies for maximizing STD performance remain uncertain. To address this problem, we identify three major steps in distillation-based STD: (i) light-to-heat energy conversion, (ii) thermal vapor generation, and (iii) conversion of vapor to water via condensation. Using specific water productivity as a quantitative metric for energy efficiency, we show that efficient recovery of the latent heat of condensation is critical for STD performance enhancement, because solar vapor generation has already been pushed toward its performance limit. We also demonstrate that STD cannot compete with photovoltaic reverse osmosis desalination in energy efficiency. We conclude by emphasizing the importance of factors other than energy efficiency, including cost, ease of maintenance, and applicability to hypersaline waters.

INTRODUCTION

The growing demand for desalination to augment water supply coupled with concerns about the environmental impacts of powering desalination using fossil fuel have spurred substantial interest in developing desalination systems that are powered by renewable energy (*1*, *2*). Tremendous interest in developing integrated solar-thermal desalination (STD) systems has emerged in the past few years, especially systems enabled by solar-driven interfacial evaporation (*3*, *4*). In these systems, there are three steps for the production of fresh water: (i) conversion of solar radiation to thermal energy (heat), (ii) utilization of the generated heat for vapor production, and (iii) condensation of the vapor to water. Most research effort in this area has been devoted to the development of high-performance materials for photothermal conversion (*5*–*11*), while system design has received growing attention (*12*–*15*).

Despite myriad efforts to develop novel materials and configurations for STD, a knowledge gap still exists in quantitative understanding of how these innovations can translate to the overall enhancement of STD performance. In particular, the vast majority of reported studies focused on vapor generation under solar radiation (*5*–*7*, *9*, *16*–*19*). While vapor generation is a critical component of STD, high-performance STD cannot be achieved without efficient condensation and effective recovery of the latent heat of condensation (*20*–*22*). Therefore, a systematic framework is needed to quantify the significance of different strategies for enhancing the efficiency of STD systems and to identify the most effective strategies to achieve high-performance STD. Such a framework is also necessary for performance evaluation of different STD systems with various materials, designs, and experimental conditions.

In this review, we critically discuss the fundamental principles of designing an efficient STD system from both material development and system design perspectives. We start by introducing a general framework for analyzing the performance of STD systems. Following this framework, we discuss the role of emerging materials in enhancing heat generation from solar radiation. We then examine different thermal management strategies for maximizing vapor generation using the heat converted from solar radiation. We also elucidate the importance of latent heat recovery and demonstrate the potential of markedly enhancing the efficiency of STD systems by implementing measures for latent heat recovery. The limitations of energy efficiency for STD systems are also discussed by comparing STD to the energy efficiency of solar desalination based on photovoltaic (PV)–driven reverse osmosis (RO). Last, we summarize the effective pathways for enhancing the efficiency of STD systems and highlight practical and economic aspects of designing STD systems.

DEFINING THE PERFORMANCE OF STD SYSTEMS

The most relevant metric for evaluating the performance of STD systems is the specific water productivity (SWP), defined as the volume of water produced per solar radiation area per time. This metric represents how efficiently the energy available from solar radiation is used to desalinate a given source water. SWP has been commonly reported as the key performance metric in numerous studies on STD (*5*, *6*, *13*, *19*–*21*, *23*–*27*). In most studies, the solar irradiance was set to one sun for practical relevance (*12*, *13*, *20*, *24*–*26*), although much higher solar irradiance has been used in some studies (*5*, *6*, *19*, *27*).

SWP can be expressed as (see the Supplementary Materials for derivation)

$$\mathrm{SWP} = \frac{E}{L}\alpha\eta_t \mathrm{GOR} \quad (1)$$

where E is the solar irradiance (kW m^{-2}), L is the latent heat of evaporation (kWh liter^{-1}), α is the solar absorptivity of the STD system (dimensionless) that quantifies the percentage of solar irradiance converted to heat, η_t is the thermal efficiency (dimensionless) that

[1]Department of Civil and Environmental Engineering, Vanderbilt University, Nashville, TN 37235, USA. [2]Department of Chemical and Environmental Engineering, Yale University, New Haven, CT 06520-8286, USA. [3]Department of Civil, Environmental, and Architectural Engineering, University of Colorado Boulder, Boulder, CO 80309, USA. [4]Department of Earth and Environmental Engineering and Columbia Water Center, Columbia University, New York, NY 10027, USA. [5]Department of Mechanical Engineering, Vanderbilt University, Nashville, TN 37235, USA. [6]Department of Chemical and Biomolecular Engineering, Vanderbilt University, Nashville, TN 37235, USA.
*Corresponding author. Email: menachem.elimelech@yale.edu (M.E.); shihong.lin@vanderbilt.edu (S.L.)

quantifies the percentage of generated heat used for evaporation, and GOR is the gained output ratio. GOR, defined as the kilogram of distilled water produced per kilogram of vapor produced, quantifies the degree to which the latent heat of condensation is reused for further distillation (*28*, *29*). Because the thermal energy required to generate 1 kilogram of vapor is constant, GOR is a measure of energy efficiency of thermal distillation. The GOR of a well-designed thermal distillation system should be notably greater than unity.

We call Eq. 1 the governing equation for STD systems, as it applies to all STD systems regardless of specific system design. This governing equation is of fundamental importance because it provides a clear theoretical and quantitative framework for understanding how the overall performance of STD systems, as quantified by the SWP, can be enhanced by improving the performance of the three important conversion processes (Fig. 1). Specifically, the first process converts solar radiation to thermal energy, the second process generates vapor (or steam) using heat, and the third process converts vapor to water. The efficiencies of these three conversion processes are quantified by solar absorptivity (α), thermal efficiency (η_t), and GOR, respectively. We will organize the following discussion according to the structure of this governing equation and analyze how the performance of each conversion process can be enhanced by recent or future research efforts.

MATERIALS FOR HIGH SOLAR-THERMAL CONVERSION EFFICIENCY

To achieve high SWP, it is imperative to have a solar absorber with high absorptivity (α). Because α is defined as the ratio of the total absorbed irradiance to the total received solar irradiance (Fig. 2A), materials with high absorptivity must effectively absorb light throughout the solar spectrum (*7*, *16*, *30*, *31*). These materials should behave like a blackbody, absorbing nearly all incident radiation with little reflection and transmission. Two major categories of materials have been widely considered as highly effective solar absorbers: carbonaceous materials and plasmonic nanoparticles.

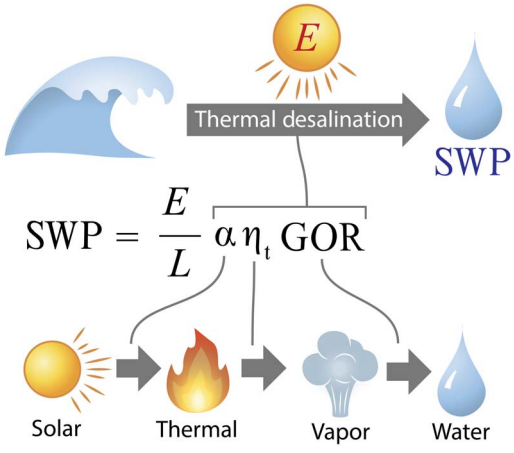

Fig. 1. Key factors in efficient STD systems. The governing equation for distillation-based STD, with the SWP as the performance metric. The impact of three important parameters—solar absorptivity (α), thermal efficiency (η_t), and GOR—on SWP is illustrated. The three thick arrows denote three independent steps: (i) conversion of solar energy to thermal energy by solar absorber, (ii) generation of vapor using the thermal energy, and (iii) production of water from vapor through condensation and latent heat recovery.

Carbonaceous materials are inherently suitable for broadband absorption owing to the π-band's optical transitions (*32*–*34*). The optically excited electrons can quickly relax via thermalization due to electron-electron and electron-phonon scattering. Both conventional bulk carbon materials, such as carbon black (CB) (*35*–*37*) and graphite (*14*, *38*), and carbonaceous nanomaterials, such as graphene (*27*, *39*, *40*), graphene oxide (GO) (*25*, *26*, *41*–*43*), and carbon nanotubes (CNTs) (*44*, *45*), have been used for constructing solar absorbers with high absorptivity (Fig. 2B). Natural organic structures, such as wood stem and mushroom, have also been carbonized to become effective solar absorbers (*46*–*48*).

The second category of solar absorbers attracting tremendous recent attention is based on nanoscale plasmonic resonance with near-perfect light-to-heat conversion efficiency (Fig. 2C) (*8*, *49*–*52*). However, plasmonic nanoparticles of a certain size can only effectively absorb radiation with a narrow bandwidth. To achieve broadband photothermal conversion, size-distributed plasmonic nanoparticles (e.g., Au or Al) have been packed into porous structures to fabricate plasmonic absorbers with overall absorptivity beyond 95% or, in extreme cases, reaching 99% (*5*, *6*, *19*). Such an ultrahigh full-spectrum absorptivity is attributable to the intense hybridized surface plasmon resonance across the assembled nanoparticles with distributed sizes and multiple scattering within submicrometer-scale pores (Fig. 2C).

Beyond these two major categories, other materials have also been explored as effective solar absorbers, such as surfaces coated with polydopamine (*53*), black TiO_2 nanoparticles (*11*, *54*), or other metal oxide nanoparticles (*16*, *17*). The microscopic structures of several selected highly efficient solar absorbers in this category reported in recent studies are shown in Fig. 2D. Polydopamine-coated solar absorbers are biodegradable and thereby environmentally friendly (*53*), while solar absorbers with metal oxide nanoparticle coating are stable and durable for practical applications (*16*, *17*, *54*).

The absorptivities of selected solar absorbers reported in recent studies (*5*, *6*, *19*, *25*, *37*, *46*, *48*, *54*, *55*) and that of several common natural and engineered surfaces (*56*–*59*) are presented in Fig. 2E. In general, novel solar absorber materials exhibit higher solar absorptivity compared to natural surfaces. For instance, the solar absorptivity of natural surfaces, such as wood and leaves, is lower than 55% (*37*, *46*), whereas carbonaceous absorbers, including CB-coated polyacrylonitrile (PAN) membranes, GO films, and carbonized mushrooms, have solar absorptivities greater than 90% (*14*, *37*, *48*). In addition, some plasmonic-based solar absorbers, such as Au-plasmonic absorber and Pd-plasmonic wood, display nearly perfect solar absorptivity, approaching 100% (*5*, *6*).

Burgeoning recent research in manipulating nanoscale materials and structures has shown a myriad of material possibilities to fabricate very "dark" surfaces and, in certain cases, advanced our fundamental understanding of photothermal conversion. However, as can be seen in Fig. 2E, commercially available materials such as CB paints and black chrome can already reach an absorptivity over 90% and have been used widely in solar collectors (*36*, *37*, *56*). Therefore, future development of novel materials for photothermal conversion should not simply focus on further enhancing absorptivity but must be justified by cost and sustainability. For example, carbonization of very low cost natural materials and structures may be promising for fabricating scalable, economical, and highly efficient porous solar absorbers.

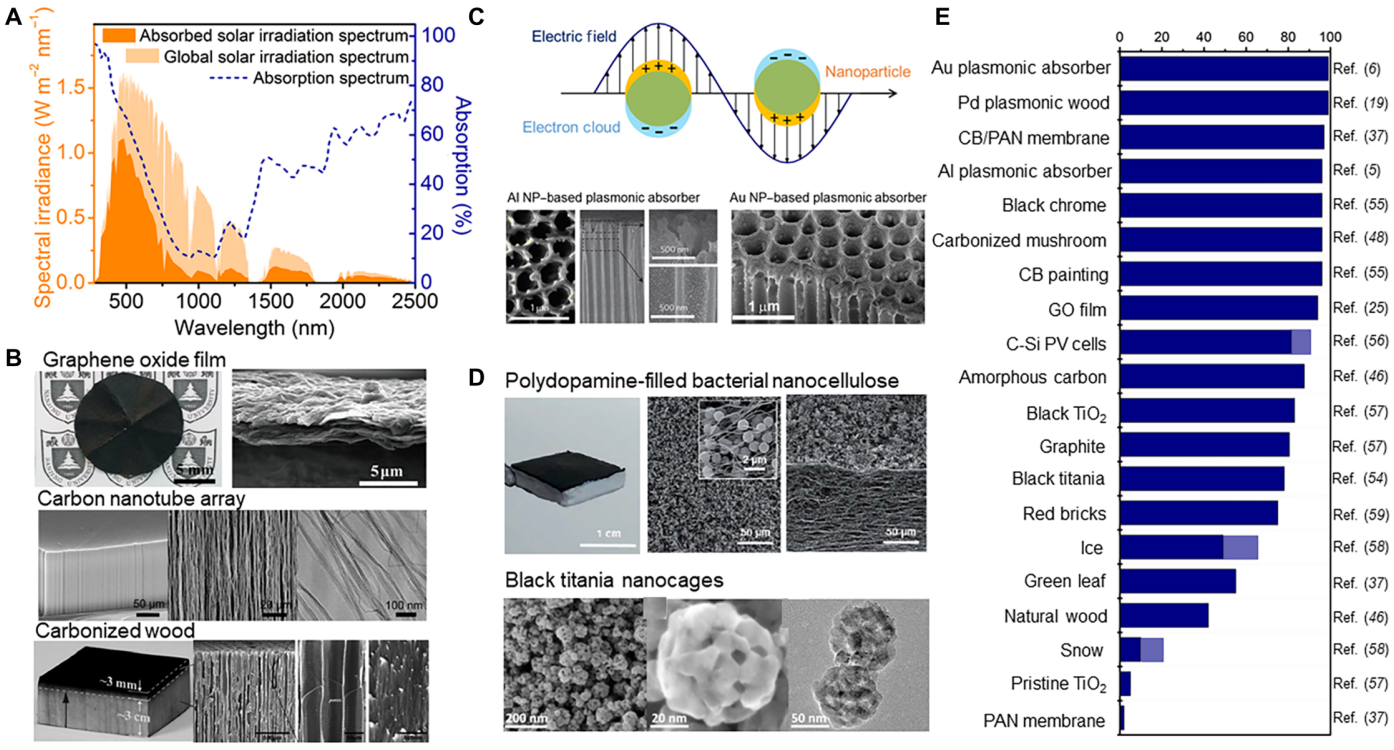

Fig. 2. Solar absorber design principles and representative examples. (**A**) Solar absorption (dark blue dashed line) and absorbed solar irradiance (solid orange area) spectra of natural wood (as an example) as a function of light wavelength (*46*). The transparent orange area represents the global solar radiation spectrum. (**B**) Carbonaceous materials-based solar absorbers including GO films (*25*), CNT arrays (*44*), and carbonized wood (*46*). Reproduced with permissions from the National Academy of Sciences (*25*), the American Chemical Society (*44*), and John Wiley and Sons (*46*). (**C**) Plasmonic materials to maximize solar radiation absorption made from aluminum nanoparticles (Al NPs) (*5*) and gold nanoparticles (Au NPs) (*6*). Reproduced with permissions from Springer Nature (*5*) and the American Association for the Advancement of Science (*6*). The extremely high solar absorptivity of the plasmonic materials is due to localized surface plasmon resonance enabled by size-distributed nanoparticles. (**D**) Examples of other developed solar absorbers, including polydopamine-filled bacterial nanocellulose (*53*) and black titania nanocage films (*54*). Reproduced with permissions from the Royal Society of Chemistry (*53*) and the American Chemical Society (*54*). (**E**) Solar absorptivity (α) of selected materials (*5*, *6*, *19*, *25*, *37*, *46*, *48*, *54*–*59*). The solid blue columns denote the absorptivity values; the absorptivity values of some materials are within a certain range as indicated by the transparent blue columns.

THERMAL MANAGEMENT STRATEGIES FOR EFFICIENT VAPOR GENERATION FROM HEAT

In an STD process, not all the absorbed solar energy can be used for vapor generation because of parasitic heat losses due to thermal radiation, convection, and conduction (Fig. 3A) (*12*, *41*, *60*). We define thermal efficiency (η_t) as the effectiveness of using the heat generated from photothermal conversion for water evaporation in an STD process. On the basis of the governing equation for STD performance (i.e., Eq. 1), a high η_t is required to attain a high SWP. Therefore, effective thermal management must be implemented to minimize parasitic heat losses.

One of the most commonly reported thermal management strategies is to reduce conductive heat loss to the feed saline water by minimizing the direct contact between the solar absorber and the feed solution (*25*, *38*). This is typically achieved using hydrophilic "wicks" to transport water to a porous solar absorber (Fig. 3B). A modification of this scheme with the same principle is the use of a good thermal insulator with capillary channels (e.g., foam and wood) between the absorber and bulk saline water (*13*, *24*, *47*, *61*–*63*). By separating the solar absorber and bulk solution with such a thermally insulating layer, the heat loss to the bulk solution by conduction can be substantially reduced.

Another effective thermal management strategy is to use a selective absorber that can minimize thermal radiation heat loss to the air (Fig. 3C). For a nonselective blackbody absorber with high solar absorptivity α, the emissivity ε is also high according to Kirchhoff's law (ε = α) (*64*), which consequently leads to substantial heat loss due to thermal radiation and reduces the amount of heat available for vapor generation. Because the peak wavelength (λ) of thermal radiation is notably higher than the solar spectrum (350 to 4000 nm), thermal radiation can be mitigated using a selective absorber with a stepwise absorptivity/emissivity (i.e., $\alpha = \varepsilon = 1$ for $\lambda < 4000$ nm and $\alpha = \varepsilon = 0$ for $\lambda \geq 4000$ nm). Following this principle, selective absorbers have been prepared by applying optical coatings to nonselective broad-spectrum absorbers (*65*–*68*). Such a selective solar absorber has been recently used for developing a high-performance STD system (*12*). We note that the selective solar absorber does not function as desired when it is submerged in water or even when there is a thin water film on its surface, as in these cases the thermal radiation is dependent on the emissivity of water (~0.98) (*69*). This situation can be circumvented either by having a hydrophobic top layer for simple vapor generators (*3*, *23*, *32*, *35*, *38*) or by using nonporous solar absorbers in a way similar to a conventional solar-thermal water heater (*20*, *70*).

To further elucidate the significance of these thermal management strategies and the impacts of solar absorptivity and system configuration on thermal efficiency, η_t, energy balance analysis is performed for several steady-state systems with different configurations by considering thermal radiation, convective heat transfer to head space, conductive

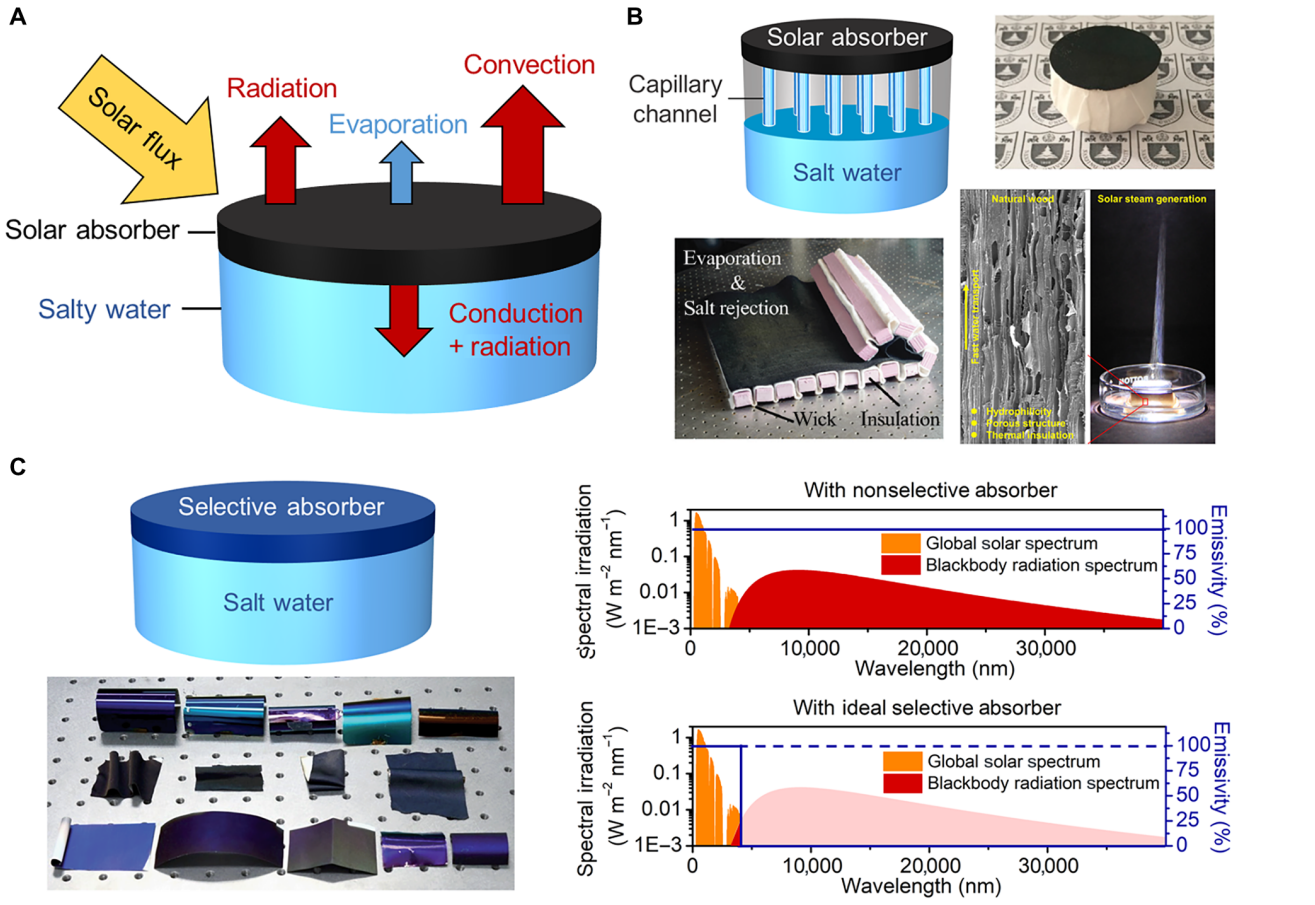

Fig. 3. Thermal management strategies in STD systems. (**A**) Schematic of energy balance in an STD system. The yellow arrow represents the absorbed solar flux; the three red arrows denote the energy losses by conduction, radiation, and convection; the blue arrow refers to the energy for effective water evaporation. (**B**) Schematic and examples of capillary channels (wick mechanism) that reduce heat loss to the bulk saline solution. Different foams (*24*, *25*) and wood (*47*) have been used to enable the wick mechanism in STD systems. Reproduced with permissions from the Royal Society of Chemistry (*24*), the National Academy of Sciences (*25*), and Elsevier (*47*). (**C**) Schematic and examples of selective solar absorbers that minimize radiation heat loss (*66*). Reproduced with permission from the Royal Society of Chemistry (*66*). Comparison of a nonselective absorber and an ideal selective absorber is shown on the right. The orange and red regions denote the solar and blackbody spectra, respectively, while the dark blue curve represents the emissivity of the solar absorber. The blackbody radiation spectrum was estimated using Planck's law of blackbody radiation with a solar absorber temperature of 373 K (*133*).

heat transfer to feed water, and heat transfer due to water evaporation. Details of the energy balance analysis are presented in the Supplementary Materials. The average absorber temperature and the distribution of the incident solar radiation (i.e., for water evaporation and various heat dissipations) are plotted as a function of solar absorptivity for different system configurations (Fig. 4).

In the first scenario, a nonselective absorber with wavelength-independent absorptivity is placed on top of the saline feed solution in a thermally insulated reservoir (Fig. 4A). Once the system reaches steady state, no further heat is transferred to the feed water because of the lack of temperature gradient between the solar absorber and the already hot saline water. While thermal insulation of the feed water reservoir is typically not practiced in most recent laboratory studies of STD, it can be readily implemented in real STD systems (*71*, *72*). As can be seen in Fig. 4A, a large fraction of the adsorbed radiation is used for vapor generation (i.e., high η_t), whereas a small fraction is lost through convection to the head space and thermal radiation. In addition, despite the nearly linear dependence of steady-state absorber temperature on solar absorptivity, α, as indicated by the temperature profile (dashed black curve in Fig. 4A), a weak dependence of η_t on α is observed, because the ratio of the evaporation energy (blue region) to the total absorbed solar irradiance (sum of blue, purple, and red regions) is nearly independent of α. These results suggest that the impact of α is mainly on how much heat is generated but not on how the generated heat is used. We also observe that the steady-state temperature of the system is quite low (less than 45°C with $\alpha = 1$), which is consistent with reported studies (*13*, *24*, *61*, *73*, *74*).

In the second scenario (Fig. 4B), the nonselective absorber with wavelength-independent absorptivity is replaced by a selective absorber with step-function absorptivity/emissivity (as in Fig. 3C). With the selective absorber (Fig. 4B), the steady-state radiative heat loss (red region) is negligible compared to that of the nonselective absorber (Fig. 4A). Furthermore, due to the elimination of radiative heat loss, both the absorber temperature (dashed black curve) and energy used for evaporation (blue region) in the second scenario (Fig. 4B) are enhanced compared to those in the first scenario (Fig. 4A). Our analysis confirms that selective absorbers can effectively increase η_t by eliminating most of the radiative heat loss.

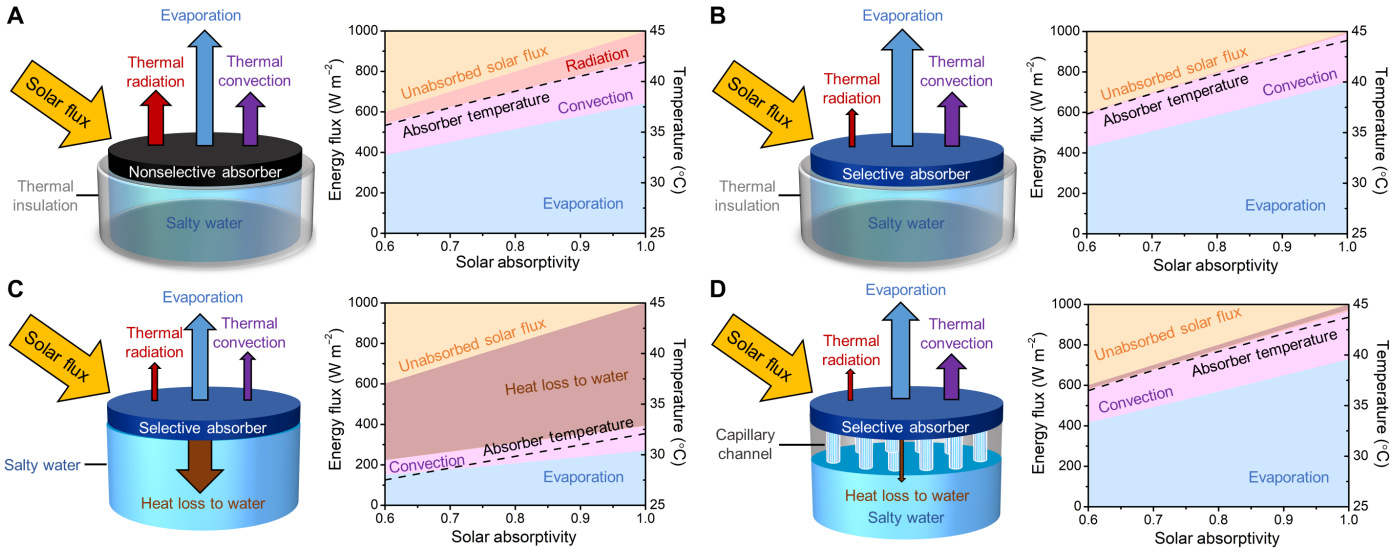

Fig. 4. Energy balance analysis in STD systems. Energy balance analysis is performed in four different steady-state STD configurations: (**A**) a nonselective absorber with a finite bulk solution volume with perfect thermal insulation, (**B**) a selective absorber with a finite bulk solution volume with perfect thermal insulation, (**C**) a selective absorber with an infinite bulk solution volume and no wick, and (**D**) a selective absorber with an infinite bulk solution volume and wick. For each scenario, the energy flux and temperature of the absorber as a function of the solar absorptivity (α) of the absorber are also plotted next to the schematic of each STD configuration. In each plot, the total incoming solar flux is 1000 W m^{-2}, and it is equal to the sum of the unabsorbed solar flux (orange region), the radiative heat loss (red region), the convective heat loss (purple region), the heat loss to water (brown region), and the energy consumption for evaporation (blue region). The dashed black curve represents the average temperature of the absorber.

STD systems have been proposed for direct placement on the surface of natural waters (e.g., lakes and oceans) as floating systems (*20*, *24*, *61*, *73*). Hence, we also analyze a scenario in which the feed water solution is infinitely large and of constant temperature (Fig. 4C). In this case, heat loss to feed water via conduction becomes very notable, as recognized by several previous studies (*12*, *24*, *37*, *61*, *75*). Specifically, the heat loss to feed water (brown region) comprises more than half of the heat generated from solar radiation (Fig. 4C). Consequently, the steady-state temperature is also substantially lower than that for the two scenarios described in Fig 4, A and B, where the solar absorbers are coupled with a well-insulated reservoir of finite size. Our analysis indicates that placing a selective absorber directly on a large water body is inefficient because of substantial heat loss.

To mitigate the notable detrimental impact of conductive heat loss to an unconfined water reservoir, a wicking mechanism can be used to minimize the thermal contact between the solar absorber and the feed water beneath (Fig. 4D). While such a strategy has been implemented in many different forms (*3*, *4*, *24*, *25*, *47*, *61*, *75*, *76*), all forms share a similar mechanism of using hydrophilic capillaries that can effectively transport water but not heat (*3*, *12*, *25*, *38*, *74*, *76*, *77*). Depending on the system design, the space between the solar absorber and feed water can be filled with thermally insulating materials (*24*, *47*, *61*, *75*) or just be left empty (equivalent to being filled with air) (*13*, *41*, *74*), which markedly reduces heat transfer to the unconfined feed water. Consistent with most reported studies, our analysis shows that this strategy is highly effective in enhancing the overall efficiency of STD systems. The steady-state temperature and distribution of heat utilization and heat loss in this case (Fig. 4D) are similar to the case where the solar absorbers are coupled with a well-insulated heat reservoir of finite size (Fig. 4B).

It is often argued that interfacial heating is critical to high-performance STD because it allows heating only the water near the liquid-air interface instead of the entire feed water supply (*3*–*5*, *23*, *36*, *38*, *51*, *54*). While this statement is correct for floating STD systems on a lake or ocean (i.e., the volume of feed reservoir is infinite), it is theoretically questionable for on-ground STD systems with a finite volume of feed water (see analysis in the Supplementary Materials). Nonetheless, there are two practical advantages of applying interfacial heating in on-ground STD systems. The first practical advantage is the elimination of the need for excellent thermal insulation. Notably, most water reservoirs were not insulated in STD studies that demonstrated substantial performance improvement by implementing interfacial heating (*5*, *23*, *26*, *36*, *51*). The second advantage of interfacial heating is the shortening of the start-up time of evaporation as most of the heat is used at the interface (*73*, *77*), which is particularly important on partially cloudy days with intermittent solar radiation. Shortening the start-up time of vapor generation effectively results in higher SWP.

For STD systems using interfacial absorbers for direct vapor generation, besides the thermal management strategies, another factor with important influence on the overall performance of STD systems is the housing design. Two major requirements exist for a good housing for STD systems. First, the housing must promote efficient vapor condensation to prevent the head space from being saturated, as otherwise the driving force for water evaporation would be substantially reduced. This may be achieved by engineering housing material with special wettability that can promote fast dropwise condensation (*78*–*81*); however, the condensation surface must be designed in such a way that condensed droplets do not fall back to the feed water. The use of solar-powered electric fans to force convection has also been proposed to promote condensation (*81*, *82*). Second, the housing material should have high transmissivity to solar radiation for a high overall absorptivity of the STD system. We note that the SWP reported in most STD studies [with a few exceptions (*20*, *21*, *24*, *61*, *73*)] was measured for the vapor generation alone without condensation. Future research should quantitatively examine the impact of housing design on the overall

SWP of interfacial STD systems and provide guidance for the design of cost-effective housing that works synergistically with high-performance solar absorbers to deliver the best STD performance.

THE CRITICAL NEED FOR EFFICIENT LATENT HEAT RECOVERY

The above analysis suggests that the efficiency of generating vapor using solar-thermal energy may have a limit, mostly because of the parasitic heat losses that undermine the thermal efficiency for vapor generation, η_t. Moreover, the potential improvement of SWP is rather limited because $\alpha\eta_t$ is theoretically capped by unity (i.e., $\alpha\eta_t \leq 1$). In contrast, as we can see from Eq. 1, there is a notably larger opportunity for improving SWP by enhancing the GOR. The GOR roughly quantifies the number of times the latent heat is reused and can be over 15 for well-engineered, facility-scale thermal desalination systems (*83*, *84*). Here, we will use a few examples to illustrate how engineered thermal desalination systems can be coupled with solar-thermal collectors to construct STD systems with very high SWP.

For large-scale STD systems, the simplest system configuration involves connecting a conventional multistage flash (MSF) or multiple-effect distillation (MED) system with an external solar heater (*85*–*87*). MSF and MED are mature thermal desalination technologies with capacity or flow rate ranging from 10^2 to 10^6 m^3 day^{-1}. Readers can find more detailed descriptions of MSF and MED in other publications (*88*–*90*). Although different in system configuration, MSF and MED are both designed to facilitate the recovery of the latent heat of condensation (Fig. 5A). Fast evaporation even at relatively low temperatures is achieved in MSF or MED by reducing the pressure of the head space, which, in turn, leads to boiling point reduction (*91*). To maintain partial vacuum, only a small amount of electricity is consumed in practice to continuously remove the generated vapor from the system. For example, the overall specific energy consumption (SEC) in the form of electrical input typically ranges from 2 to 5 kWh m^{-3}, which is a small fraction of the specific thermal energy consumption (*83*, *92*, *93*).

The average temperature of the feed stream and that of the distillate (or condensate) stream in each stage dictates the vapor pressure at the respective liquid-air interfaces, which, in turn, determines the driving force for distillation. Therefore, it is necessary to maintain a reasonable temperature difference between the feed and distillate streams to achieve an acceptable water vapor flux (*91*). This requirement of finite temperature difference in each stage implies that only a finite number

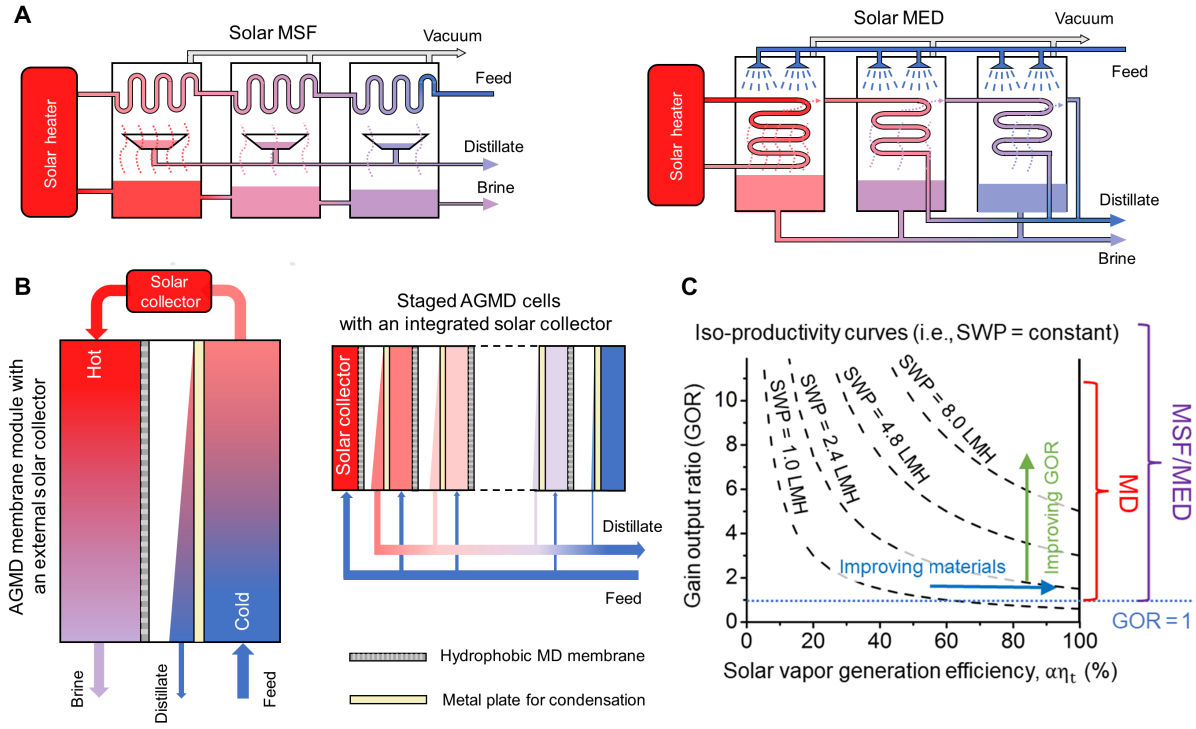

Fig. 5. Methods for recovering the latent heat of vaporization in solar-thermal distillation systems. (**A**) MSF distillation (left) and MED driven by solar-thermal energy. (**B**) AGMD coupled with an external solar heater (left) and AGMD with solar heater integrated to the membrane module or to the MD membrane (right). For AGMD coupled with an external solar heater (left), the latent heat of evaporation can be efficiently recovered as the feed water is warmed by the heat released from vapor condensation in the air chamber before entering the solar heater. Similarly, for AGMD with solar heater integrated in the membrane module (right), latent heat recovery can be achieved by using staged cells. In the first stage, the feed water is heated by the absorbed solar energy, and from the second stage on, the feed water is heated by the latent heat released from vapor condensation in the air chamber of the previous stage. (**C**) Impacts of the GOR and solar vapor generation efficiency, $\alpha\eta_t$, on the SWP. By definition, SWP is the volume of water produced per solar radiation area (i.e., the area of solar absorber facing the sun) per time. The black dashed curves are the iso-productivity curves, along which the SWP is constant. Currently, in most studies of STD systems, the GOR is 1 (blue dotted line), and the goal is to increase SWP by enhancing $\alpha\eta_t$ (blue arrow). The red and purple parentheses on the right axis refer to the achievable GOR of MD and MSF/MED systems, respectively (*96*, *134*). The green arrow shows the potential of increasing SWP by enhancing GOR. Solar irradiance is assumed to be 1000 W m^{-2}. The units for SWP are in liters m^{-2} $hour^{-1}$ (LMH).

of stages can be implemented for a given feed temperature. Because the GOR is strongly dependent on the number of stages, it may be desirable to enhance the temperature at the solar heater so that a large number of stages can be practically implemented. This may be achieved with parabolic solar concentrators to increase the areal power of the radiation (*94*, *95*). However, this approach does not necessarily enhance the SWP if the area used in defining SWP is the area for receiving solar radiation but not the area for receiving the concentrated radiation.

While MSF and MED are mature and highly efficient thermal desalination technologies, they are not practical or economically viable for small-scale applications. A potential technology to be used in small-scale STD is membrane distillation (MD) (*96*, *97*). In an MD process, the hot (saline) feed stream is separated from the cold (distillate) stream by a hydrophobic porous MD membrane. The temperature difference generates a partial vapor pressure difference across the MD membrane, which provides the driving force for vapor transport. There are several major system configurations for MD, including direct contact MD (DCMD), air-gap MD (AGMD), sweeping gas MD (SGMD), and vacuum MD (VMD) (*98*, *99*). While each configuration has its own advantages, AGMD (Fig. 5B, left) has unique advantages for developing small-scale STD systems (*100*, *101*).

In a solar thermal AGMD system, the same saline feed water is circulated through the feed chamber and the cooling water chamber in a counter-current flow system. The vapor transferred across the MD membrane enters the distillate chamber and condenses on a thermally conductive condensation surface in contact with a cooling stream, producing distillate that can be collected as product water. The cold feed stream is warmed by collecting the latent heat of condensation transferred from the hot feed stream via conduction and then absorbs additional heat from the solar thermal collector to become the hot feed stream. The counter-current configuration facilitates the recovery of latent heat. The use of saline feed water as the cooling stream is particularly advantageous for small-scale STD systems because it eliminates the need for a large volume of fresh water to initiate the process. In addition, with AGMD configuration, heat recovery is inherently built in, thus eliminating the need for an additional heat exchanger for heat recovery as required in DCMD (*102*, *103*).

Integration of photothermal conversion material onto the surface of the MD membrane has recently been proposed for enhancing the efficiency of DCMD systems (*104*, *105*). Here, the efficiency enhancement is defined as the reduction in the consumption of externally supplied heat that is not from solar-thermal conversion. These solar-heated MD membranes can also be used in AGMD systems, which do not require distilled water to initiate operation as in DCMD systems (*106*, *107*). Because direct solar heating on an MD membrane creates a homogeneously hot membrane surface, a potentially better configuration is multistage AGMD in which the latent heat of condensation from one stage drives the evaporation in the next stage (Fig. 5B, right). Unlike AGMD powered by external solar heating (Fig. 5B, left), which behaves like a heat exchanger with a strong temperature gradient along the flow direction, multistage AGMD with a built-in solar heating MD membrane theoretically has no temperature gradient along the membrane surface. Instead, a temperature difference exists between stages. A similar STD configuration using the principle of MD has also been developed by replacing the top layer of the system. Specifically, the MD membrane with integrated photothermal conversion materials was replaced by a composite film of commercial solar-thermal absorber (top), a thin wicking film (intermediate), and a hydrophobic MD membrane (bottom) (*20*).

One important advantage of multistage integrated MD systems with a solar-thermal heating top layer is the possible elimination of a water pump, as each feed chamber can simply be filled with porous, hydrophilic wicking materials that spontaneously and continuously absorb feed water from the reservoir (*108*). This advantage is particularly important for small-scale, low-cost STD systems, because it enables a pump-free, passive system that does not require an extra PV panel to generate electricity. The lack of electrical components with moving parts also reduces the risk of system failure. Moreover, compared to AGMD with an external solar heater, multistage integrated MD systems eliminate the need for external heaters.

With either external or integrated solar heating, the concept of GOR can be applied to evaluate the performance of an AGMD system (*109*, *110*). While more in-depth modeling of these systems is needed to acquire comprehensive and quantitative understanding of system energy efficiency, the GOR of these systems is strongly dependent on the temperature difference across the MD membrane and the air gap, ΔT. For AGMD with external solar heating, the average ΔT is dependent on the effective membrane area for a given circulation flow rate, which is similar to the behavior of a heat exchanger. A larger membrane area results in a smaller average ΔT, which leads to a lower vapor flux but less required external heat input. For multistage integrated MD systems, the average ΔT is dependent on the number of stages, which is also proportional to the total membrane area installed. More distillate will be generated as the number of stages increases, but the average vapor flux will also decrease as more stages lead to reduced driving force for each stage. In either case, a higher GOR can be achieved by increasing the total membrane area of the AGMD system, which inevitably increases the capital cost.

The substantial impact of GOR on the overall system performance as quantified by SWP is demonstrated by the governing equation for STD (Eq. 1 and Fig. 1) and further illustrated using iso-productivity curves (Fig. 5C) generated using Eq. 1. An iso-productivity curve is a set of GOR and $\alpha\eta_t$ values that lead to the same SWP, with $\alpha\eta_t$ quantifying the efficiency of using solar radiation for generating vapor. Without latent heat recovery (i.e., GOR = 1), increasing $\alpha\eta_t$ to its maximum (i.e., 100%) can only lead to a relatively marginal improvement of SWP (Fig. 5C). Thus, developments of high-performance materials and structures for solar-thermal vapor generation can only improve the overall system performance to a limited extent. The results in Fig. 5C convincingly show that the much more rewarding direction to enhance system performance is to substantially increase GOR, which can lead to multifold enhancement of SWP. This has been experimentally confirmed in a recent study in which the SWP was enhanced by sixfold using a passive 10-stage integrated MD system (*20*). Achieving a GOR over 10 or even 15 is technically feasible but not with small-scale, low-cost thermal desalination systems (*96*).

Substantial progress has been made to date to improve the solar vapor generation efficiency (i.e., fabricating novel solar absorbers with high α and application of rational thermal management strategies to maximize η_t). Nevertheless, consequential challenges and future opportunities lie in developing effective, low-cost measures for latent heat recovery that can be implemented in STD systems, particularly in small- to medium-scale systems. For instance, in an STD system with no latent heat recovery (GOR = 1), the SWP is capped at about 1.6 liters m^{-2} $hour^{-1}$ with a perfect solar vapor generation efficiency of 100% (Fig. 5C). In comparison, if some low-cost measures can be implemented in the STD system to effectively increase the GOR just to

3, then the SWP can be readily elevated to nearly 4 liters m^{-2} $hour^{-1}$ with a practical solar vapor generation efficiency of 80%. Our analysis suggests that cost-effective measures for latent heat recovery can lead to leapfrog improvement of STD performance that cannot be matched by perfecting materials and structures for solar vapor generation.

INHERENT LIMITATIONS OF STD

While SWP can be substantially improved by enhancing the GOR by maximizing latent heat recovery, it is important to realize that STD, however optimized, is unlikely to be the most energy-efficient way to harness solar energy for desalination. This is because thermal desalination processes are inherently substantially less energy efficient than RO, the state-of-the-art desalination technology (*96*). For example, for desalination of seawater, which has a salinity of around 35 g $liter^{-1}$, typical RO plants consume about 3 to 4 kWh to produce 1 m^3 of product water, i.e., the specific energy consumption (SEC) is 3 to 4 kWh m^{-3} (10.8 to 14.4 MJ m^{-3}) (*111*, *112*). This SEC includes energy needs for water intake, pretreatment, desalination by RO, and post-treatment. The actual energy spent in the RO stage with a typical water recovery of 50% is ~2 kWh m^{-3} (7.2 MJ m^{-3}), which is remarkably close to the energy consumption of an ideal constant-pressure RO process (1.6 kWh m^{-3}) and a thermodynamically reversible variable-pressure RO process (1.1 kWh m^{-3}) (*1*, *113*). In fact, the energy consumption of the RO separation step is within a factor of 3 of the ultimate thermodynamic limit, achieved with a near-zero water recovery (of 0.76 kWh m^{-3} or ~2.74 MJ m^{-3}). Compared to pressure-driven RO, any evaporation-based thermal desalination process consumes substantially more energy. For example, conventional thermal distillation processes consume a staggering ~2260 MJ m^{-3} (628 kWh m^{-3}, GOR = 1) to ~151 MJ m^{-3} (42 kWh m^{-3}, GOR = ~15), which is one to more than two orders of magnitude higher than that of RO (*83*). This SEC is only representative of the thermal energy input and does not include the additional electrical energy consumed by pumps to maintain vacuum or circulate the feed and brine streams.

The marked difference in SEC between RO and thermal distillation has a fundamental thermodynamic origin (*1*, *96*). The minimum SEC required for desalination is the specific Gibbs free energy of separation, Δg. From a thermodynamic perspective, Δg is the minimum energy required to reduce the entropy of the system from its initial state (i.e., feed water) to its final state (i.e., concentrated brine and deionized product water). In an RO process, most of the energy is directly used for water/salt separation. Therefore, the SEC of RO is on the same order of magnitude as Δg, even if the system is not operated as a thermodynamically reversible process. For distillation processes, however, the thermal energy is spent to provide the latent heat of evaporation (i.e., for phase change), which is nearly three orders of magnitude higher than Δg (*114*, *115*). This explains mechanistically why recovering latent heat is of critical importance for enhancing the energy efficiency of thermal distillation processes. However, there are limits for latent heat recovery in practical thermal distillation processes with a finite desalination rate (*91*). Even with a GOR of 15, which can only be achieved in very large scale systems with many stages or effects, the SEC of thermal distillation is still more than an order of magnitude larger than that for RO (*83*).

With this fundamental understanding of SEC for different desalination processes, we now consider its impact on the SWP, which is the core performance metric in solar desalination. SWP is proportional to the solar energy utilization efficiency, η_s ($=\alpha\eta_t$), and inversely proportional to the SEC (see Eq. S1 in the Supplementary Materials). For a well-designed STD system with excellent photothermal conversion and thermal management, η_s may vary from 60% to over 90% in the most ideal cases (*63*, *77*, *116*, *117*). However, SEC for thermal desalination is high, ranging from 151 MJ m^{-3} (42 kWh m^{-3}), with the best-performing MED systems with a GOR of 15, to ~2260 MJ m^{-3} (628 kWh m^{-3}) in the absence of any latent heat recovery (i.e., GOR = 1) (*83*, *96*). Combining these ranges of η_s and SEC, the SWP under one sun ranges from ~1.0 liter m^{-2} $hour^{-1}$, typical of solar stills (*118*, *119*), to slightly over 20 liters m^2 $hour^{-1}$, which we consider a practical limit for STD with current state-of-the-art technologies (Fig. 6, purple region).

In comparison, a PV-RO process can yield substantially higher SWP. We note that η_s for solar electricity generation using PV panels is much lower than η_s for solar-thermal generation. Typical η_s for commercially available solar cells ranges from 12 to 25%, whereas the best-performing multijunction cells can even reach a remarkable efficiency beyond 45% (*120*). Here, we use a range of 12 to 25% for η_s in calculating SWP. The SEC for RO strongly depends on the feed salinity and water recovery, with higher feed salinity and water recovery both leading to a higher SEC. For our analysis, we chose a range of SEC between 2 and 4 kWh m^{-3} (*1*, *113*), noting that much lower values are also possible with brackish water desalination. With these ranges of η_s and SEC, the calculated range of SWP is 30 to 125 liters m^{-2} $hour^{-1}$ (Fig. 6, green region). Notably, the best-performing PV-RO systems using commercially available components can yield an SWP that is two orders of magnitude higher than that of a simple solar still without latent heat recovery. Even a conservative PV-RO system is likely to yield a higher SWP than the most advanced STD system with an η_s of 95% and a GOR of 15.

The above analysis demonstrates that PV-RO systems outperform distillation-based STD systems in terms of SWP. However, the analysis does not necessarily mean that solar desalination should always be

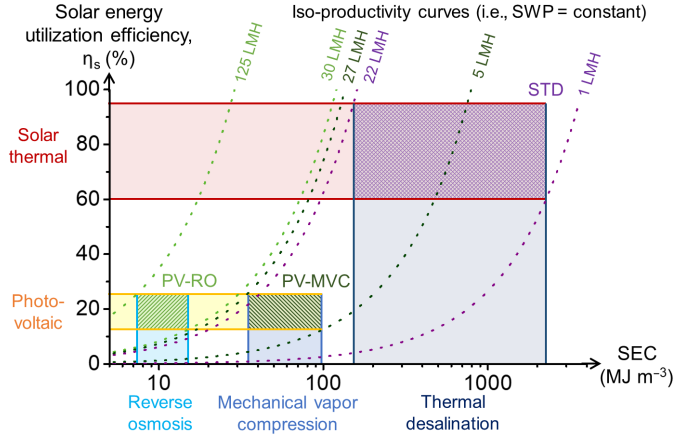

Fig. 6. Solar utilization efficiency and SEC in thermal and nonthermal desalination systems. The operating regimes are defined by solar energy utilization efficiency ($\eta_s = \alpha\eta_t$, vertical axis) and SEC (horizontal axis) for STD (purple region), PV-MVC (dark green region), and PV-RO (green region). The dotted curves denote the iso-productivity curves of constant SWPs. The limits of SWP for the three regions are given by the iso-productivity curves bypassing the corners of the regions. Specifically, the green, dark green, and purple dotted curves refer to the limits of SWP for PV-RO, PV-MVC, and STD, respectively. Solar irradiance is assumed to be 1000 W m^{-2}. The units for SWP are in liters m^{-2} $hour^{-1}$ (LMH).

pursued using PV-RO instead of thermal approaches. RO systems cannot currently be applied for treating high-salinity streams because of the limit on the allowable working pressure (*121*, *122*). The applied pressure in RO must exceed the osmotic pressure of the brine. The typical working pressure of seawater RO processes is below 85 bar, which means that conventional RO cannot be used to treat brines with salinity greater than 70 g/liter (*123*, *124*). RO with working pressures up to 300 bar has been recently proposed for concentrating a hypersaline brine stream (*125*). However, this high-pressure RO is currently not available due to the lack of pumps, membranes, and membrane modules that can operate at such high-pressure conditions. In contrast to RO, thermal distillation is not constrained by the brine salinity and can push desalination to the limit of salt crystallization (*126*, *127*). Therefore, thermally driven desalination is one of the few options for desalinating hypersaline feed solutions and/or for achieving an ultrahigh water recovery. This is necessary when treating hypersaline shale gas–produced water, concentrating brine streams from in-land desalination, and achieving zero liquid discharge (*121*, *123*, *128*).

Another possible option for using solar energy to treat hypersaline brine is to use PV-generated electricity to power mechanical vapor compression (MVC). In an MVC process, electricity is consumed to compress the vapor and elevate the vapor temperature. Latent heat recovery in MVC is very efficient, yielding an SEC in the range from 9.4 to 26.4 kWh m^{-3} (33.8 to 95.0 MJ m^{-3}) for seawater desalination (*93*, *129*, *130*). It is important to note that although MVC is mechanistically a thermal desalination process, its only energy input is electricity. Powered by commercially available PV panels with η_s varying from 12 to 25%, the SWP in PV-MVC systems ranges from 5 to 27 liters m^{-2} $hour^{-1}$ (Fig. 6, dark green region), which overlaps with the range of SWP for STD. Because of the higher η_s of STD, an ideal STD with a high degree of latent heat recovery may achieve SWP similar to that achieved by a PV-MVC with good performance.

Cost is another aspect that may favor STD over PV-RO and PV-MVC in certain scenarios (*86*, *131*, *132*). For decentralized applications, such as generating drinking water for individual households or supplying water to very small communities in remote regions, capital cost and ease of maintenance are important factors to consider. SWP, although being the core performance metric in a technical analysis, may not have substantial importance, especially in scenarios where land use is not a limiting factor. A solar desalination system with very low SWP may require a much larger area of solar radiation to achieve the same total water productivity delivered by another more efficient solar desalination system with a much higher SWP. However, the former can be economically justified if its overall cost is lower for achieving the same total water productivity and if occupying more land is not a practical concern. In this regard, simple, low-cost, low-maintenance STD systems with low SWP may be justified over not only more efficient but also more expensive and maintenance-intensive PV-RO or STD systems that are based on advanced thermal desalination processes such as MSF or MED.

OUTLOOK

In this review, we present a theoretical framework for evaluating the SWP—defined as the volume of water produced per area of solar radiation per time—of solar desalination systems. On the basis of this framework, we show that SWP is dependent on how efficiently solar energy is used for vapor generation and to what extent latent heat is recovered. Most existing work on STD focused on enhancing the efficiency of solar energy utilization (η_s) by increasing the absorptivity of solar absorbers (α) and thermal efficiency of vapor generation (η_t). To date, η_s values greater than 90% have been achieved in advanced STD systems. However, the potential for further improvement of η_s is very limited, as η_s ($=\alpha\eta_t$) is capped at 100%. Hence, future development of novel solar-absorbing materials should focus on the use of sustainable materials with reduced cost and environmental impact rather than pushing the limit of solar energy utilization efficiency. Because commercially available solar absorbers can already achieve an absorptivity greater than 90%, new solar absorbers can be justified only if they are substantially cheaper and more environmentally sustainable.

For a simple, single-stage STD system with no heat recovery, more attention should be paid to housing design for efficient vapor condensation. Failure to achieve efficient condensation will compromise the efficiency of solar energy utilization and offset the benefit of fast evaporation. However, the much more rewarding direction for further enhancing the SWP of STD systems is to improve the GOR by implementing effective measures for latent heat recovery. A very high GOR (over 15) can be achieved in mature thermal distillation technologies such as MSF and MED, but these processes are inefficient as small-scale systems and typically require high capital cost. Therefore, simpler and more cost-effective measures of latent heat recovery need to be developed for substantial improvement of the SWP of small-scale STD systems. For this purpose, MD and its variants have been actively explored and have demonstrated a GOR of up to 6 using small, passive MD-based STD devices.

We also discuss why even the most efficient STD systems cannot achieve an SWP comparable to that obtained with PV-RO. Although the collection of solar thermal energy can achieve a much higher efficiency of solar energy utilization than generating electricity using PV panels, this advantage of STD is dwarfed by its major limitation: reliance upon thermal desalination processes that are inherently less energy efficient than the pressure-driven RO process. This advantage of PV-RO in energy efficiency is unlikely to be challenged by any future improvement of STD system design, especially as better PV technologies reach the market.

Our discussion and analysis lead to a more holistic roadmap for the adoption and future development of STD. If the objective is to achieve a very high SWP, then STD systems would not be competitive with PV-RO. In fact, almost all newly built large-scale desalination plants are based on RO technology because of its superior energy efficiency, which, in turn, contributes to the overall cost advantage of RO compared to thermal desalination processes such as MSF and MED. Changing the energy source to solar energy will unlikely affect the comparative advantages of RO over MSF or MED for large-scale desalination plants. STD, however, may be justified for treating hypersaline brines that are beyond the current capability of RO but will also have to compete with PV-MVC in this application domain.

STD would be most attractive for low-demand, distributed solar desalination in remote and underdeveloped areas where water demand is not high and land use is not a critical constraint. In these applications, SWP will have much less practical relevance, and other factors, such as capital cost and ease of maintenance, would be critically important. Given these considerations, active STD systems based on MSF or MED cannot compete with simple, passive STD systems even if the latter have substantially lower SWP. While latent heat recovery is of crucial significance for enhancing the SWP, whether and to what extent it should be implemented in simple, passive STD systems eventually depends on the trade-off between SWP and capital cost.

SUPPLEMENTARY MATERIALS

Supplementary material for this article is available at http://advances.sciencemag.org/cgi/content/full/5/7/eaax0763/DC1

Fig. S1. Schematic of energy fluxes in an STD system at steady state.

Table S1. Parameters for the energy balance analysis.

References (*135*–*137*)

REFERENCE AND NOTES

1. M. Elimelech, W. A. Phillip, The future of seawater desalination: Energy, technology, and the environment. *Science* **333**, 712–717 (2011).
2. N. Ghaffour, J. Bundschuh, H. Mahmoudi, M. F. A. Goosen, Renewable energy-driven desalination technologies: A comprehensive review on challenges and potential applications of integrated systems. *Desalination* **356**, 94–114 (2015).
3. P. Tao, G. Ni, C. Song, W. Shang, J. Wu, J. Zhu, G. Chen, T. Deng, Solar-driven interfacial evaporation. *Nat. Energy* **3**, 1031–1041 (2018).
4. P. Wang, Emerging investigator series: The rise of nano-enabled photothermal materials for water evaporation and clean water production by sunlight. *Environ. Sci. Nano* **5**, 1078–1089 (2018).
5. L. Zhou, Y. Tan, J. Wang, W. Xu, Y. Yuan, W. Cai, S. Zhu, J. Zhu, 3D self-assembly of aluminium nanoparticles for plasmon-enhanced solar desalination. *Nat. Photonics* **10**, 393–398 (2016).
6. L. Zhou, Y. Tan, D. Ji, B. Zhu, P. Zhang, J. Xu, Q. Gan, Z. Yu, J. Zhu, Self-assembly of highly efficient, broadband plasmonic absorbers for solar steam generation. *Sci. Adv.* **2**, e1501227 (2016).
7. K. Bae, G. Kang, S. K. Cho, W. Park, K. Kim, W. J. Padilla, Flexible thin-film black gold membranes with ultrabroadband plasmonic nanofocusing for efficient solar vapour generation. *Nat. Commun.* **6**, 10103 (2015).
8. M. S. Zielinski, J.-W. Choi, T. La Grange, M. Modestino, S. M. H. Hashemi, Y. Pu, S. Birkhold, J. A. Hubbell, D. Psaltis, Hollow mesoporous plasmonic nanoshells for enhanced solar vapor generation. *Nano Lett.* **16**, 2159–2167 (2016).
9. L. Zhang, J. Xing, X. Wen, J. Chai, S. Wang, Q. Xiong, Plasmonic heating from indium nanoparticles on a floating microporous membrane for enhanced solar seawater desalination. *Nanoscale* **9**, 12843–12849 (2017).
10. L. Yi, S. Ci, S. Luo, P. Shao, Y. Hou, Z. Wen, Scalable and low-cost synthesis of black amorphous Al-Ti-O nanostructure for high-efficient photothermal desalination. *Nano Energy* **41**, 600–608 (2017).
11. M. Ye, J. Jia, Z. Wu, C. Qian, R. Chen, P. G. O'Brien, W. Sun, Y. Dong, G. A. Ozin, Synthesis of black TiO_x nanoparticles by Mg reduction of TiO_2 nanocrystals and their application for solar water evaporation. *Adv. Energy Mater.* **7**, 1601811 (2017).
12. G. Ni, G. Li, S. V. Boriskina, H. Li, W. Yang, T. Zhang, G. Chen, Steam generation under one sun enabled by a floating structure with thermal concentration. *Nat. Energy* **1**, 16126 (2016).
13. Y. Li, T. Gao, Z. Yang, C. Chen, W. Luo, J. Song, E. Hitz, C. Jia, Y. Zhou, B. Liu, B. Yang, L. Hu, 3D-printed, all-in-one evaporator for high-efficiency solar steam generation under 1 sun illumination. *Adv. Mater.* **29**, 1700981 (2017).
14. V. Kashyap, A. Al-Bayati, S. M. Sajadi, P. Irajizad, S. H. Wang, H. Ghasemi, A flexible anti-clogging graphite film for scalable solar desalination by heat localization. *J. Mater. Chem. A* **5**, 15227–15234 (2017).
15. F. Zhao, X. Zhou, Y. Shi, X. Qian, M. Alexander, X. Zhao, S. Mendez, R. Yang, L. Qu, G. Yu, Highly efficient solar vapour generation via hierarchically nanostructured gels. *Nat. Nanotechnol.* **13**, 489–495 (2018).
16. Y. Shi, R. Li, Y. Jin, S. Zhuo, L. Shi, J. Chang, S. Hong, K.-C. Ng, P. Wang, A 3D photothermal structure toward improved energy efficiency in solar steam generation. *Joule* **2**, 1171–1186 (2018).
17. Y. Shi, R. Li, L. Shi, E. Ahmed, Y. Jin, P. Wang, A robust $CuCr_2O_4/SiO_2$ composite photothermal material with underwater black property and extremely high thermal stability for solar-driven water evaporation. *Adv. Sustainable Syst.* **2**, 1700145 (2018).
18. H. Ren, M. Tang, B. Guan, K. Wang, J. Yang, F. Wang, M. Wang, J. Shan, Z. Chen, D. Wei, H. Peng, Z. Liu, Hierarchical graphene foam for efficient omnidirectional solar-thermal energy conversion. *Adv. Mater.* **29**, 1702590 (2017).
19. M. Zhu, Y. Li, F. Chen, X. Zhu, J. Dai, Y. Li, Z. Yang, X. Yan, J. Song, Y. Wang, E. Hitz, W. Luo, M. Lu, B. Yang, L. Hu, Plasmonic wood for high-efficiency solar steam generation. *Adv. Energy Mater.* **8**, 1701028 (2018).
20. E. Chiavazzo, M. Morciano, F. Viglino, M. Fasano, P. Asinari, Passive solar high-yield seawater desalination by modular and low-cost distillation. *Nat. Sustain.* **1**, 763–772 (2018).
21. G. Xue, Q. Chen, S. Lin, J. Duan, P. Yang, K. Liu, J. Li, J. Zhou, Highly efficient water harvesting with optimized solar thermal membrane distillation device. *Glob. Chall.* **2**, 1800001 (2018).
22. J. M. Gordon, H. T. Chua, The merits of plasmonic desalination. *Nat. Photonics* **11**, 70 (2017).
23. L. Zhang, B. Tang, J. Wu, R. Li, P. Wang, Hydrophobic light-to-heat conversion membranes with self-healing ability for interfacial solar heating. *Adv. Mater.* **27**, 4889–4894 (2015).
24. G. Ni, S. H. Zandavi, S. M. Javid, S. V. Boriskina, T. A. Cooper, G. Chen, A salt-rejecting floating solar still for low-cost desalination. *Energy Environ. Sci.* **11**, 1510–1519 (2018).
25. X. Li, W. Xu, M. Tang, L. Zhou, B. Zhu, S. Zhu, J. Zhu, Graphene oxide-based efficient and scalable solar desalination under one sun with a confined 2D water path. *Proc. Natl. Acad. Sci. U.S.A.* **113**, 13953–13958 (2016).
26. X. Hu, W. Xu, L. Zhou, Y. Tan, Y. Wang, S. Zhu, J. Zhu, Tailoring graphene oxide-based aerogels for efficient solar steam generation under one sun. *Adv. Mater.* **29**, 1604031 (2017).
27. P. Zhang, J. Li, L. Lv, Y. Zhao, L. Qu, Vertically aligned graphene sheets membrane for highly efficient solar thermal generation of clean water. *ACS Nano* **11**, 5087–5093 (2017).
28. R. L. McGinnis, M. Elimelech, Energy requirements of ammonia–carbon dioxide forward osmosis desalination. *Desalination* **207**, 370–382 (2007).
29. J. Tonner, *Barriers to Thermal Desalination in the United States* (U.S. Department of the Interior, Bureau of Reclamation, 2008).
30. T. Lin, C. Yang, Z. Wang, H. Yin, X. Lu, F. Huang, J. Lin, X. Xie, M. Jiang, Effective nonmetal incorporation in black titania with enhanced solar energy utilization. *Energ. Environ. Sci.* **7**, 967–972 (2014).
31. M. Gao, L. Zhu, C. K. Peh, G. W. Gim, Solar absorber material and system designs for photothermal water vaporization towards clean water and energy production. *Energy Environ. Sci.* **12**, 841–864 (2019).
32. V.-D. Dao, H.-S. Choi, Carbon-based sunlight absorbers in solar-driven steam generation devices. *Glob. Chall.* **2**, 1700094 (2018).
33. K. Mizuno, J. Ishii, H. Kishida, Y. Hayamizu, S. Yasuda, D. N. Futaba, M. Yumura, K. Hata, A black body absorber from vertically aligned single-walled carbon nanotubes. *Proc. Natl. Acad. Sci. U.S.A.* **106**, 6044–6047 (2009).
34. A. B. Kuzmenko, E. van Heumen, F. Carbone, D. van der Marel, Universal optical conductance of graphite. *Phys. Rev. Lett.* **100**, 117401 (2008).
35. W. Xu, X. Hu, S. Zhuang, Y. Wang, X. Li, L. Zhou, S. Zhu, J. Zhu, Flexible and salt resistant Janus absorbers by electrospinning for stable and efficient solar desalination. *Adv. Energy Mater.* **8**, 1702884 (2018).
36. Y. Liu, J. Chen, D. Guo, M. Cao, L. Jiang, Floatable, self-cleaning, and carbon-black-based superhydrophobic gauze for the solar evaporation enhancement at the air–water interface. *ACS Appl. Mater. Interfaces* **7**, 13645–13652 (2015).
37. S. Zhuang, L. Zhou, W. Xu, N. Xu, X. Hu, X. Li, G. Lv, Q. Zheng, S. Zhu, Z. Wang, J. Zhu, Tuning transpiration by interfacial solar absorber-leaf engineering. *Adv. Sci.* **5**, 1700497 (2018).
38. H. Ghasemi, G. Ni, A. M. Marconnet, J. Loomis, S. Yerci, N. Miljkovic, G. Chen, Solar steam generation by heat localization. *Nat. Commun.* **5**, 4449 (2014).
39. Y. Yang, R. Zhao, T. Zhang, K. Zhao, P. Xiao, Y. Ma, P. Ajayan, G. Shi, Y. Chen, Graphene-based standalone solar energy converter for water desalination and purification. *ACS Nano* **12**, 829–835 (2018).
40. Y. Ito, Y. Tanabe, J. Han, T. Fujita, K. Tanigaki, M. Chen, Multifunctional porous graphene for high-efficiency steam generation by heat localization. *Adv. Mater.* **27**, 4302–4307 (2015).
41. C. Finnerty, L. Zhang, D. L. Sedlak, K. L. Nelson, B. Mi, Synthetic graphene oxide leaf for solar desalination with zero liquid discharge. *Environ. Sci. Technol.* **51**, 11701–11709 (2017).
42. G. Wang, Y. Fu, A. Guo, T. Mei, J. Wang, J. Li, X. Wang, Reduced graphene oxide–polyurethane nanocomposite foam as a reusable photoreceiver for efficient solar steam generation. *Chem. Mater.* **29**, 5629–5635 (2017).
43. N. Yousefi, X. Lu, M. Elimelech, N. Tufenkji, Environmental performance of graphene-based 3D macrostructures. *Nat. Nanotechnol.* **14**, 107–119 (2019).
44. Z. Yin, H. Wang, M. Jian, Y. Li, K. Xia, M. Zhang, C. Wang, Q. Wang, M. Ma, Q.-s. Zheng, Y. Zhang, Extremely black vertically aligned carbon nanotube arrays for solar steam generation. *ACS Appl. Mater. Interfaces* **9**, 28596–28603 (2017).
45. C. Chen, Y. Li, J. Song, Z. Yang, Y. Kuang, E. Hitz, C. Jia, A. Gong, F. Jiang, J. Y. Zhu, B. Yang, J. Xie, L. Hu, Highly flexible and efficient solar steam generation device. *Adv. Mater.* **29**, 1701756 (2017).
46. M. Zhu, Y. Li, G. Chen, F. Jiang, Z. Yang, X. Luo, Y. Wang, S. D. Lacey, J. Dai, C. Wang, C. Jia, J. Wan, Y. Yao, A. Gong, B. Yang, Z. Yu, S. Das, L. Hu, Tree-inspired design for high-efficiency water extraction. *Adv. Mater.* **29**, 1704107 (2017).
47. C. Jia, Y. Li, Z. Yang, G. Chen, Y. Yao, F. Jiang, Y. Kuang, G. Pastel, H. Xie, B. Yang, S. Das, L. Hu, Rich mesostructures derived from natural woods for solar steam generation. *Joule* **1**, 588–599 (2017).
48. N. Xu, X. Hu, W. Xu, X. Li, L. Zhou, S. Zhu, J. Zhu, Mushrooms as efficient solar steam-generation devices. *Adv. Mater.* **29**, 1606762 (2017).
49. M. L. Brongersma, N. J. Halas, P. Nordlander, Plasmon-induced hot carrier science and technology. *Nat. Nanotechnol.* **10**, 25–34 (2015).

50. H. H. Richardson, M. T. Carlson, P. J. Tandler, P. Hernandez, A. O. Govorov, Experimental and theoretical studies of light-to-heat conversion and collective heating effects in metal nanoparticle solutions. *Nano Lett.* **9**, 1139–1146 (2009).
51. Z. Wang, Y. Liu, P. Tao, Q. Shen, N. Yi, F. Zhang, Q. Liu, C. Song, D. Zhang, W. Shang, T. Deng, Bio-inspired evaporation through plasmonic film of nanoparticles at the air-water interface. *Small* **10**, 3234–3239 (2014).
52. M. Gao, P. K. N. Connor, G. W. Ho, Plasmonic photothermic directed broadband sunlight harnessing for seawater catalysis and desalination. *Energ. Environ. Sci.* **9**, 3151–3160 (2016).
53. Q. Jiang, H. G. Derami, D. Ghim, S. Cao, Y.-S. Jun, S. Singamaneni, Polydopamine-filled bacterial nanocellulose as a biodegradable interfacial photothermal evaporator for highly efficient solar steam generation. *J. Mater. Chem. A* **5**, 18397–18402 (2017).
54. G. Zhu, J. Xu, W. Zhao, F. Huang, Constructing black titania with unique nanocage structure for solar desalination. *ACS Appl. Mater. Interfaces* **8**, 31716–31721 (2016).
55. J. Wang, Y. Li, L. Deng, N. Wei, Y. Weng, S. Dong, D. Qi, J. Qiu, X. Chen, T. Wu, High-performance photothermal conversion of narrow-bandgap Ti_2O_3 nanoparticles. *Adv. Mater.* **29**, 1603730 (2017).
56. J. H. Henninger, *Solar Absorptance and Thermal Emittance of Some Common Spacecraft Thermal-Control Coatings* (NASA, 1984).
57. R. Santbergen, R. J. C. van Zolingen, The absorption factor of crystalline silicon PV cells: A numerical and experimental study. *Sol. Energy Mater. Sol. Cells* **92**, 432–444 (2008).
58. P. K. Munneke, Snow, ice and solar radiation. Thesis, Utrecht University (2009).
59. J. Yao, C. Yan, Effects of solar absorption coefficient of external wall on building energy consumption. *Int. J. Civil Environ. Eng.* **5**, 208–210 (2011).
60. X. Wang, Y. He, X. Liu, G. Cheng, J. Zhu, Solar steam generation through bio-inspired interface heating of broadband-absorbing plasmonic membranes. *Appl. Energy* **195**, 414–425 (2017).
61. Z. Liu, H. Song, D. Ji, C. Li, A. Cheney, Y. Liu, N. Zhang, X. Zeng, B. Chen, J. Gao, Y. Li, X. Liu, D. Aga, S. Jiang, Z. Yu, Q. Gan, Extremely cost-effective and efficient solar vapor generation under nonconcentrated illumination using thermally isolated black paper. *Glob. Chall.* **1**, 1600003 (2017).
62. K.-K. Liu, Q. Jiang, S. Tadepallifit, R. Raliya, P. Biswas, R. R. Naik, S. Singamaneni, Wood–graphene oxide composite for highly efficient solar steam generation and desalination. *ACS Appl. Mater. Interfaces* **9**, 7675–7681 (2017).
63. X. Yin, Y. Zhang, Q. Guo, X. Cai, J. Xiao, Z. Ding, J. Yang, Macroporous double-network hydrogel for high-efficiency solar steam generation under 1 sun illumination. *ACS Appl. Mater. Interfaces* **10**, 10998–11007 (2018).
64. F. E. Nicodemu, Directional reflectance and emissivity of an opaque surface. *Appl. Optics* **4**, 767–775 (1965).
65. F. Cao, K. McEnaney, G. Chen, Z. Ren, A review of cermet-based spectrally selective solar absorbers. *Energy Environ. Sci.* **7**, 1615–1627 (2014).
66. F. Chen, S.-W. Wang, X. Liu, R. Ji, L. Yu, X. Chen, W. Lu, High performance colored selective absorbers for architecturally integrated solar applications. *J. Mater. Chem. A* **3**, 7353–7360 (2015).
67. S. R. Atchuta, S. Sakthivel, H. C. Barshilia, Transition metal based $Cu_xNi_yCo_{z-x-y}O_4$ spinel composite solar selective absorber coatings for concentrated solar thermal applications. *Sol. Energy Mater. Sol. Cells* **189**, 226–232 (2019).
68. A. A. Günay, H. Kim, N. Nagarajan, M. Lopez, R. Kantharaj, A. Alsaati, A. Marconnet, A. Lenert, N. Miljkovic, Optically transparent thermally insulating silica aerogels for solar thermal insulation. *ACS Appl. Mater. Interfaces* **10**, 12603–12611 (2018).
69. W. G. Rees, S. P. James, Angular variation of the infrared emissivity of ice and water surfaces. *Int. J. Remote Sens.* **13**, 2873–2886 (1992).
70. M. Al-harahsheh, M. Abu-Arabi, H. Mousa, Z. Alzghoul, Solar desalination using solar still enhanced by external solar collector and PCM. *Appl. Therm. Eng.* **128**, 1030–1040 (2018).
71. M. Chandrashekara, A. Yadav, Water desalination system using solar heat: A review. *Renew. Sustain. Energy Rev.* **67**, 1308–1330 (2017).
72. M. Abu-Arabi, M. Al-harahsheh, H. Mousa, Z. Alzghoul, Theoretical investigation of solar desalination with solar still having phase change material and connected to a solar collector. *Desalination* **448**, 60–68 (2018).
73. L. Zhu, M. Gao, C. K. N. Peh, X. Wang, G. W. Ho, Self-contained monolithic carbon sponges for solar-driven interfacial water evaporation distillation and electricity generation. *Adv. Energy Mater.* **8**, 1702149 (2018).
74. H. Liu, X. Zhang, Z. Hong, Z. Pu, Q. Yao, J. Shi, G. Yang, B. Mi, B. Yang, X. Liu, H. Jiang, X. Hu, A bioinspired capillary-driven pump for solar vapor generation. *Nano Energy* **42**, 115–121 (2017).
75. T. Li, H. Liu, X. Zhao, G. Chen, J. Dai, G. Pastel, C. Jia, C. Chen, E. Hitz, D. Siddhartha, R. Yang, L. Hu, Scalable and highly efficient mesoporous wood-based solar steam generation device: Localized heat, rapid water transport. *Adv. Funct. Mater.* **28**, 1707134 (2018).
76. Y. Liu, S. Yu, R. Feng, A. Bernard, Y. Liu, Y. Zhang, H. Duan, W. Shang, P. Tao, C. Song, T. Deng, A bioinspired, reusable, paper-based system for high-performance large-scale evaporation. *Adv. Mater.* **27**, 2768–2774 (2015).
77. Z. Wang, Q. Ye, X. Liang, J. Xu, C. Chang, C. Song, W. Shang, J. Wu, P. Tao, T. Deng, Paper-based membranes on silicone floaters for efficient and fast solar-driven interfacial evaporation under one sun. *J. Mater. Chem. A* **5**, 16359–16368 (2017).
78. R. Enright, N. Miljkovic, J. L. Alvarado, K. Kim, J. W. Rose, Dropwise condensation on micro- and nanostructured surfaces. *Nanosc. Microsc. Therm.* **18**, 223–250 (2014).
79. X. Chen, J. Wu, R. Ma, M. Hua, N. Koratkar, S. Yao, Z. Wang, Nanograssed micropyramidal architectures for continuous dropwise condensation. *Adv. Funct. Mater.* **21**, 4617–4623 (2011).
80. H. J. Cho, D. J. Preston, Y. Zhu, E. N. Wang, Nanoengineered materials for liquid-vapour phase-change heat transfer. *Nat. Rev. Mater.* **2**, 16092 (2017).
81. Y. Hou, M. Yu, X. Chen, Z. Wang, S. Yao, Recurrent filmwise and dropwise condensation on a beetle mimetic surface. *ACS Nano* **9**, 71–81 (2015).
82. P. Durkaieswaran, K. K. Murugavel, Various special designs of single basin passive solar still—A review. *Renew. Sustain. Energy Rev.* **49**, 1048–1060 (2015).
83. A. Al-Karaghouli, L. L. Kazmerski, Energy consumption and water production cost of conventional and renewable-energy-powered desalination processes. *Renew. Sustain. Energy Rev.* **24**, 343–356 (2013).
84. S. Sadri, M. Ameri, R. H. Khoshkhoo, Multi-objective optimization of MED-TVC-RO hybrid desalination system based on the irreversibility concept. *Desalination* **402**, 97–108 (2017).
85. I. Khoshrou, M. R. J. Nasr, K. Bakhtari, New opportunities in mass and energy consumption of the multi-stage flash distillation type of brackish water desalination process. *Sol. Energy* **153**, 115–125 (2017).
86. H. Sharon, K. S. Reddy, A review of solar energy driven desalination technologies. *Renew. Sustain. Energy Rev.* **41**, 1080–1118 (2015).
87. P. Palenzuela, G. Zaragoza, D. C. Alarcón-Padilla, Characterisation of the coupling of multi-effect distillation plants to concentrating solar power plants. *Energy* **82**, 986–995 (2015).
88. M. Al-Shammiri, M. Safar, Multi-effect distillation plants: State of the art. *Desalination* **126**, 45–59 (1999).
89. A. H. Khan, *Desalination Processes and Multistage Flash Distillation Practice* (Elsevier, 1986).
90. H. T. El-Dessouky, H. M. Ettouney, Y. Al-Roumi, Multi-stage flash desalination: Present and future outlook. *Chem. Eng. J.* **73**, 173–190 (1999).
91. D. Brogioli, F. La Mantia, N. Y. Yip, Thermodynamic analysis and energy efficiency of thermal desalination processes. *Desalination* **428**, 29–39 (2018).
92. S. Ihm, O. Y. Al-Najdi, O. A. Hamed, G. Jun, H. Chung, Energy cost comparison between MSF, MED and SWRO: Case studies for dual purpose plants. *Desalination* **397**, 116–125 (2016).
93. M. Al-Sahali, H. Ettouney, Developments in thermal desalination processes: Design, energy, and costing aspects. *Desalination* **214**, 227–240 (2007).
94. A. Fernández-García, E. Zarza, L. Valenzuela, M. Pérez, Parabolic-trough solar collectors and their applications. *Renew. Sustain. Energy Rev.* **14**, 1695–1721 (2010).
95. M. Elashmawy, An experimental investigation of a parabolic concentrator solar tracking system integrated with a tubular solar still. *Desalination* **411**, 1–8 (2017).
96. A. Deshmukh, C. Boo, V. Karanikola, S. Lin, A. P. Straub, T. Tong, D. M. Warsinger, M. Elimelech, Membrane distillation at the water-energy nexus: Limits, opportunities, and challenges. *Energy Environ. Sci.* **11**, 1177–1196 (2018).
97. N. Ghaffour, T. M. Missimer, G. L. Amy, Technical review and evaluation of the economics of water desalination: Current and future challenges for better water supply sustainability. *Desalination* **309**, 197–207 (2013).
98. P. Wang, T.-S. Chung, Recent advances in membrane distillation processes: Membrane development, configuration design and application exploring. *J. Membr. Sci.* **474**, 39–56 (2015).
99. M. S. El-Bourawi, Z. Ding, R. Ma, M. Khayet, A framework for better understanding membrane distillation separation process. *J. Membr. Sci.* **285**, 4–29 (2006).
100. R. B. Saffarini, E. K. Summers, H. A. Arafat, J. H. Lienhard, Technical evaluation of stand-alone solar powered membrane distillation systems. *Desalination* **286**, 332–341 (2012).
101. J. B. Gálvez, L. García-Rodríguez, I. Martín-Mateos, Seawater desalination by an innovative solar-powered membrane distillation system: The MEDESOL project. *Desalination* **246**, 567–576 (2009).
102. H. C. Duong, P. Cooper, B. Nelemans, T. Y. Cath, L. D. Nghiem, Evaluating energy consumption of air gap membrane distillation for seawater desalination at pilot scale level. *Sep. Purif. Technol.* **166**, 55–62 (2016).
103. K. Yao, Y. Qin, Y. Yuan, L. Liu, F. He, Y. Wu, A continuous-effect membrane distillation process based on hollow fiber AGMD module with internal latent-heat recovery. *AIChE J.* **59**, 1278–1297 (2013).
104. P. D. Dongare, A. Alabastri, S. Pedersen, K. R. Zodrow, N. J. Hogan, O. Neumann, J. Wu, T. Wang, A. Deshmukh, M. Elimelech, Q. Li, P. Nordlander, N. J. Halas, Nanophotonics-enabled solar membrane distillation for off-grid water purification. *Proc. Natl. Acad. Sci. U.S.A.* **114**, 6936–6941 (2017).

105. J. Wu, K. R. Zodrow, P. B. Szemraj, Q. Li, Photothermal nanocomposite membranes for direct solar membrane distillation. *J. Mater. Chem. A* **5**, 23712–23719 (2017).
106. M. A. E.-R. Abu-Zeid, Y. Zhang, H. Dong, L. Zhang, H.-L. Chen, L. Hou, A comprehensive review of vacuum membrane distillation technique. *Desalination* **356**, 1–14 (2015).
107. R. Bahar, M. N. A. Hawlader, T. F. Ariff, Channeled coolant plate: A new method to enhance freshwater production from an air gap membrane distillation (AGMD) desalination unit. *Desalination* **359**, 71–81 (2015).
108. H. Zheng, Chapter 5. Active solar distiller, in *Solar Energy Desalination Technology*, H. Zheng, Ed. (Elsevier, 2017), pp. 323–445.
109. J. Swaminathan, H. W. Chung, D. M. Warsinger, J. H. Lienhard, Membrane distillation model based on heat exchanger theory and configuration comparison. *Appl. Energy* **184**, 491–505 (2016).
110. I. Hitsov, K. De Sitter, C. Dotremont, P. Cauwenberg, I. Nopens, Full-scale validated air gap membrane distillation (AGMD) model without calibration parameters. *J. Membr. Sci.* **533**, 309–320 (2017).
111. C. Fritzmann, J. Löwenberg, T. Wintgens, T. Melin, State-of-the-art of reverse osmosis desalination. *Desalination* **216**, 1–76 (2007).
112. G. Raluy, L. Serra, J. Uche, Life cycle assessment of MSF, MED and RO desalination technologies. *Energy* **31**, 2361–2372 (2006).
113. B. Peñate, L. García-Rodríguez, Current trends and future prospects in the design of seawater reverse osmosis desalination technology. *Desalination* **284**, 1–8 (2012).
114. M. H. Sharqawy, J. H. Lienhard, S. M. Zubair, Thermophysical properties of seawater: A review of existing correlations and data. *Desalin. Water Treat.* **16**, 354–380 (2010).
115. K. S. Spiegler, Y. M. El-Sayed, The energetics of desalination processes. *Desalination* **134**, 109–128 (2001).
116. Y. Wang, C. Wang, X. Song, M. Huang, S. K. Megarajan, S. F. Shaukat, H. Jiang, Improved light-harvesting and thermal management for efficient solar-driven water evaporation using 3D photothermal cones. *J. Mater. Chem. A* **6**, 9874–9881 (2018).
117. K. Kim, S. Yu, C. An, S.-W. Kim, J.-H. Jang, Mesoporous three-dimensional graphene networks for highly efficient solar desalination under 1 sun illumination. *ACS Appl. Mater. Interfaces* **10**, 15602–15608 (2018).
118. H. Tanaka, K. Iishi, Experimental study of a vertical single-effect diffusion solar still coupled with a tilted wick still. *Desalination* **402**, 19–24 (2017).
119. R. Kalbasi, A. A. Alemrajabi, M. Afrand, Thermal modeling and analysis of single and double effect solar stills: An experimental validation. *Appl. Therm. Eng.* **129**, 1455–1465 (2018).
120. N. S. Lewis, Research opportunities to advance solar energy utilization. *Science* **351**, aad1920 (2016).
121. T. Tong, M. Elimelech, The global rise of zero liquid discharge for wastewater management: Drivers, technologies, and future directions. *Environ. Sci. Technol.* **50**, 6846–6855 (2016).
122. L. F. Greenlee, D. F. Lawler, B. D. Freeman, B. Marrot, P. Moulin, Reverse osmosis desalination: Water sources, technology, and today's challenges. *Water Res.* **43**, 2317–2348 (2009).
123. D. L. Shaffer, L. H. A. Chavez, M. Ben-Sasson, S. R.-V. Castrillón, N. Y. Yip, M. Elimelech, Desalination and reuse of high-salinity shale gas produced water: Drivers, technologies, and future directions. *Environ. Sci. Technol.* **47**, 9569–9583 (2013).
124. X. Chen, N. Y. Yip, Unlocking high-salinity desalination with cascading osmotically mediated reverse osmosis: Energy and operating pressure analysis. *Environ. Sci. Technol.* **52**, 2242–2250 (2018).
125. D. M. Davenport, A. Deshmukh, J. R. Werber, M. Elimelech, High-pressure reverse osmosis for energy-efficient hypersaline brine desalination: Current status, design considerations, and research needs. *Environ. Sci. Technol. Lett.* **5**, 467–475 (2018).
126. H. W. Chung, J. Swaminathan, D. M. Warsinger, J. H. Lienhard, Multistage vacuum membrane distillation (MSVMD) systems for high salinity applications. *J. Membr. Sci.* **497**, 128–141 (2016).
127. C. A. Quist-Jensen, F. Macedonio, D. Horbez, E. Drioli, Reclamation of sodium sulfate from industrial wastewater by using membrane distillation and membrane crystallization. *Desalination* **401**, 112–119 (2017).
128. Y. Shi, C. Zhang, R. Li, S. Zhuo, Y. Jin, L. Shi, S. Hong, J. Chang, C. Ong, P. Wang, Solar evaporator with controlled salt precipitation for zero liquid discharge desalination. *Environ. Sci. Technol.* **52**, 11822–11830 (2018).
129. D. Han, W. F. He, C. Yue, W. H. Pu, Study on desalination of zero-emission system based on mechanical vapor compression. *Appl. Energy* **185**, 1490–1496 (2017).
130. J. M. Veza, Mechanical vapour compression desalination plants—A case study. *Desalination* **101**, 1–10 (1995).
131. D. D. W. Rufuss, S. Iniyan, L. Suganthi, P. A. Davies, Solar stills: A comprehensive review of designs, performance and material advances. *Renew. Sustain. Energy Rev.* **63**, 464–496 (2016).
132. D. D. W. Rufuss, V. R. Kumar, L. Suganthi, S. Iniyan, P. A. Davies, Techno-economic analysis of solar stills using integrated fuzzy analytical hierarchy process and data envelopment analysis. *Sol. Energy* **159**, 820–833 (2018).
133. G. B. Rybicki, A. P. Lightman, *Radiative Processes in Astrophysics* (Wiley, 1979).
134. Y. Zhang, Y. Peng, S. Ji, Z. Li, P. Chen, Review of thermal efficiency and heat recycling in membrane distillation processes. *Desalination* **367**, 223–239 (2015).
135. R. Tripathi, G. N. Tiwari, Effect of water depth on internal heat and mass transfer for active solar distillation. *Desalination* **173**, 187–200 (2005).
136. V. Velmurugan, M. Gopalakrishnan, R. Raghu, K. Srithar, Single basin solar still with fin for enhancing productivity. *Energy Convers. Manage.* **49**, 2602–2608 (2008).
137. A. Hobbi, K. Siddiqui, Optimal design of a forced circulation solar water heating system for a residential unit in cold climate using TRNSYS. *Sol. Energy* **83**, 700–714 (2009).

Acknowledgments

Funding: We acknowledge support from the National Science Foundation (grant CBET 1705048) and the U.S. Department of Energy (grant DE-EE0008397). **Author contributions:** S.L., M.E., and Z.W. designed the review framework. Z.W. conducted the literature review and analysis. All the authors participated in discussion and collectively wrote the paper. **Competing interests:** The authors declare that they have no competing interests. **Data and materials availability:** All data needed to evaluate the conclusions in the paper are present in the paper and/or the Supplementary Materials. Additional data related to this paper may be requested from the authors.

Submitted 20 February 2019
Accepted 18 June 2019
Published 26 July 2019
10.1126/sciadv.aax0763

Citation: Z. Wang, T. Horseman, A. P. Straub, N. Y. Yip, D. Li, M. Elimelech, S. Lin, Pathways and challenges for efficient solar-thermal desalination. *Sci. Adv.* **5**, eaax0763 (2019).